

Received August 6, 2019, accepted September 3, 2019, date of publication September 23, 2019, date of current version October 4, 2019.

Digital Object Identifier 10.1109/ACCESS.2019.2942852

Exploiting Redundant Energy of MMC–HVDC to Enhance Frequency Response of Low Inertia AC Grid

HEEJIN KIM¹, (Member, IEEE), JAESIK KANG², (Member, IEEE),
JAE W. SHIM³, (Member, IEEE), JEF BEERTEN⁴, (Member, IEEE),
DIRK VAN HERTEM⁴, (Senior Member, IEEE), HONG-JU JUNG⁵,
CHAN-KI KIM⁶, (Senior Member, IEEE), AND KYEON HUR¹, (Senior Member, IEEE)

¹School of Electrical and Electronic Engineering, Yonsei University, Seoul 03722, South Korea

²Korea Electrotechnology Research Institute (KERI), Changwon-si 51543, South Korea

³Department of Energy Engineering, Inje University, Gimhae-si 50834, South Korea

⁴ESAT-ELECTA, Electrical Energy and Computer Architectures, KU Leuven, 3000 Leuven, Belgium

⁵Hyosung, Anyang-si 14080, South Korea

⁶KEPCO Electric Power Research Institute (KEPRI), Daejeon-si 34056, South Korea

Corresponding author: Kyeon Hur (khur@yonsei.ac.kr)

This work was supported in part by under the framework of international cooperation program managed by the National Research Foundation of Korea under Grant 2017K1A4A3013579, and in part by the Basic Science Research Program through the National Research Foundation of Korea funded by the Ministry of Education, Science and Technology under Grant 2018R1D1A1A09083054.

ABSTRACT This paper presents a grid frequency responsive inertial control for the modular multilevel converter–high voltage DC (MMC–HVDC) using the MMC design attribute, i.e. submodule redundancy for high reliability. This control does not rely on the external energy sources in providing the inertial response. With an increase in the number of levels of MMCs via the proposed n_{level} control, the submodule capacitor voltage decreases, and the electrostatic energy then flows from the submodule capacitors and supports extra power to the grid in need. Decoupled control of the AC, DC and submodule dynamics of the MMC maintains the desired control performance during and after the inertial response, emulating the inherent behavior of the synchronous machine. This study further quantifies the inertia constant of the MMC, equivalent to that of the synchronous machine. The proposed control performance is demonstrated in the context of a Jeju Island power grid with MMC–HVDC systems for the offshore wind interconnection and interconnection between mainland and Jeju. Simulation results present that the proposed method improves the frequency response in harmony with existing synchronous generators and line-commutated converter based HVDC system.

INDEX TERMS Inertia constant, maximum available energy, modular multilevel converter (MMC), n_{level} control.

I. INTRODUCTION

The loss of system inertia has become a major challenge in the future power systems due to high penetration of power electronics-based generation (e.g. photovoltaic (PV) and wind power generation), displacing fossil fuel-based synchronous generation. Sum of wind power and PV generation capacity in the EU-28 countries is already more than 20% as of 2015 and continues to increase [1]. This is a trend not only in the EU but also around the world. Recently, the Korean Government announced that the penetration level of

The associate editor coordinating the review of this manuscript and approving it for publication was Junjian Qi.

renewable energy will cover more than 20% of the total Korean electricity generation amount by 2030 [2]. This requires huge amounts (approximately 60 GW) of renewable generation units. Especially, Jeju Island, which is the biggest island in Korea, is aiming for zero carbon island, and converter-based power generation is expected to increase rapidly. The total capacity of renewable in Jeju is expected to be 2.3 GW by 2030 while the peak load demand is expected to be 1.3 GW [2]. This islanded power grid is going to check for various stability issues that can occur in low inertial power systems. The reduced inertia owing to the increased adoption of converter-interfaced renewable energy sources, which may displace incumbent synchronous generators, has a high rate

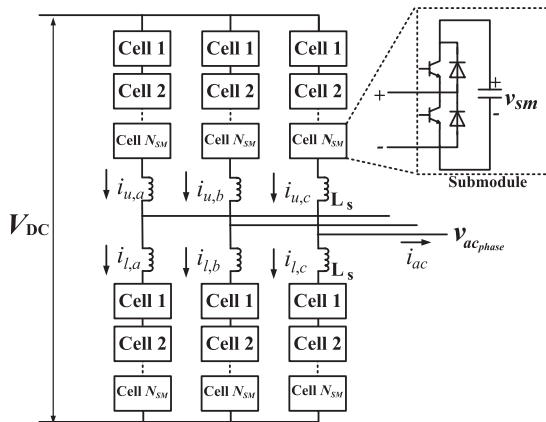


FIGURE 1. MMC basic structure.

of change of frequency (ROCOF) and reduces the damping of the electro–mechanical mode [1]. In this situation, the research efforts to improve the frequency response of power system by renewable generation and voltage–sourced converter (VSC)–high voltage direct current (HVDC) have been proposed in [3]–[20].

Over the past decade, the various research on the inertia support of wind power plant has been conducted and the inertia support and primary frequency control for provision of wind-related HVDC has been conducted [4], [5]. Inertial and primary frequency support control for multi-terminal HVDC is proposed in [3], [4]. Inertia emulation control (INEC) with DC voltage control corresponding to the AC grid frequency is proposed in [8]. Some of studies applied the characteristics of the modular multilevel converter (MMC). However, most of them used a two-level VSC.

This study develops an frequency responsive control of MMC–HVDC. The proposed method changes the number of levels in MMC control to provide inertial power to the AC grid. Contrary to the previous studies, the proposed method literally mimics the inherent and autonomous nature of the inertial response of the synchronous machines upon an event without compromising the MMC control performance after the inertial response. Furthermore, this paper calculates the amount of available energy of MMC for the frequency responsive control, and evaluates inertia constant of MMC.

Reference [7] presents an inertia support method of MMC using internal energy and the previous study assumes that the amount of energy available in the MMC is 10% of total energy stored in MMC. Unlike the previous study, this paper analytically evaluates the maximum available energy of MMC for the frequency responsive control. The submodule redundancy factor and modulation extension factor with third harmonic voltage injection are used to calculate the amount of energy that can be provided by submodules of MMC during the emergency. In addition, we examined the impact of the proposed method on the realistic power system with high penetration of the renewable generation.

II. BASIC PRINCIPLE OF MMC–HVDC

A. MMC STRUCTURE AND REDUNDANT SUBMODULE

Figure 1 illustrates a three-phase MMC–HVDC structure. The MMC consists of six arms, which are composed of a series-connected arm reactor and numerous submodules. The arm of the MMC may contain the active redundant submodules, which means that the number of submodules (N_{SM}) per arm could be different from the number of levels (N_{level}) of the MMC [22], [23]. The DC voltage (V_{DC}) of the MMC can be derived from N_{level} by multiplying the average submodule voltage ($V_{SM,avg}$) with (1), and the converter generated AC voltage varies with the modulation signal of the converter controller.

$$V_{DC} = N_{level} \times V_{SM,avg} \tag{1}$$

The number of submodules determines the stored energy in the MMC arm ($E_{arm,avg}$) as follows (2):

$$E_{arm,avg} = \frac{1}{2} C_{SM} N_{SM} \cdot V_{SM,avg}^2 \tag{2}$$

The total stored energy in the arm of an MMC is a design parameter, which determines the maximum power transfer capability [25]–[30]. Although redundant submodules improve reliability of MMC operation, the total converter loss may be increased by the conduction loss and switching loss of the redundant submodules. This study assumes that the MMC has a typical redundancy of 10% of a total number of submodules, which means that $N_{SM} \leq 1.1 \times N_{level}$.

B. MODELING AND CONTROL OF MMC–HVDC

A detailed equivalent model (DEM) of an MMC is used to achieve the inner dynamics of MMC with efficient and accurate simulation [31]–[34]. Because the MMC DEM is represented by a variable resistor and a voltage source, it reduces the computational complexity in EMT simulation. The DEM calculates the capacitor voltage for every submodule using the amount of arm current and ON/OFF state of the submodule. Thus, the total contained energy of MMC is also obtained because all the submodule capacitor voltages are known values.

The MMC–HVDC is controlled by a decoupled dq current controller. The decoupled dq current controller is used to control active power and reactive power independently.

MMC requires the submodule capacitor voltage balancing method and waveform generation method (Modulation). The capacitor voltage balancing method balances the capacitor voltages in numerous submodules of each arm. Various submodule voltage balancing methods have been proposed [35]–[38], which are classified as full-sorting or group-sorting [38]. The full-sorting method is applied for MMC–HVDC in the case study. For the waveform generation, the nearest level control (NLC) is selected among various waveform generation techniques [42] because NLC fits into the high-power, high-capacity, and high-level MMC. Thus, the number of ON submodules in each arm is obtained by

NLC as follows:

$$n_{u_j,ON} = \text{round}\left(\left((-m_j - m_{z,j}) + 1\right) \times \frac{N_{level}}{2}\right) \quad (3)$$

$$n_{l_j,ON} = \text{round}\left(\left((m_j - m_{z,j}) + 1\right) \times \frac{N_{level}}{2}\right) \quad (4)$$

where $j = a, b, c$, $n_{u_j,ON}$ is the number of ON submodules of the j phase upper arm, $n_{l_j,ON}$ is the number of ON submodules of the j phase lower arm, m_j is the modulation signal of the j phase, and $m_{z,j}$ is the common voltage modulation signal of the j phase for circulating current suppression. The range of the modulation signals (m_j and $m_{z,j}$) is between 1 and -1 .

C. AC-DC DECOUPLED CONTROL OF MMC–HVDC

To exploit the submodule energy of MMC, the AC power control and DC power control need to be separated. The submodule energy changes when the amounts of AC power and DC power of the MMC system are different from each other. Methods for AC-DC decoupled control of arm energy balancing have been proposed for MMC–HVDC [39]–[41]. AC-DC decoupled current control of MMC–HVDC with direct modulation is well studied and presented in [39], and AC-DC decoupled current control with submodule voltage feedback modulation is proposed in [40], [41]. When MMC controls AC active power and DC voltage with d -axis current control, the submodule energy is controlled by circulating common voltage control in AC-DC decoupled control. Note that AC-DC decoupled control can make submodule voltage variation. In the previous subsection II-B, we defined N_{level} as a constant value. Now, ' n_{level} control' is redefined so that the number of levels (n_{level}) is a controllable variable value, and not a constant value. When the n_{level} control is applied, equations (1), (3), and (4) is redefined as follows:

$$n_{level} = \frac{V_{DC}}{v_{SM,avg}} \quad (5)$$

$$n_{u_j,ON} = \text{round}\left(\left((-m_j - m_{z,j}) + 1\right) \times \frac{n_{level}}{2}\right) \quad (6)$$

$$n_{l_j,ON} = \text{round}\left(\left((m_j - m_{z,j}) + 1\right) \times \frac{n_{level}}{2}\right) \quad (7)$$

As can be seen in (5), as $v_{SM,avg}$ decreases, n_{level} increases. The structure of MMC controller with modified circulating current controller is depicted in Figure 2. P_{ac}^* is the desired active power, i_d^* is the desired d -axis AC current, v_{sm}^* is the desired submodule voltage, V_{DC}^* is the desired DC voltage, $i_{u,j}$ is the upper arm current of the j phase, $i_{l,j}$ is the lower arm current of the j phase, $i_{cir,d}$ is the d -axis circulating current, $i_{cir,q}$ is the q -axis circulating current, $i_{cir,o}$ is the common circulating current, $m_{z,d}$ is the d -axis modulation signal, $m_{z,q}$ is the q -axis modulation signal, $m_{z,o}$ is the common voltage modulation signal, K_p is the proportional gain, and K_i is the integral gain in Figure 2.

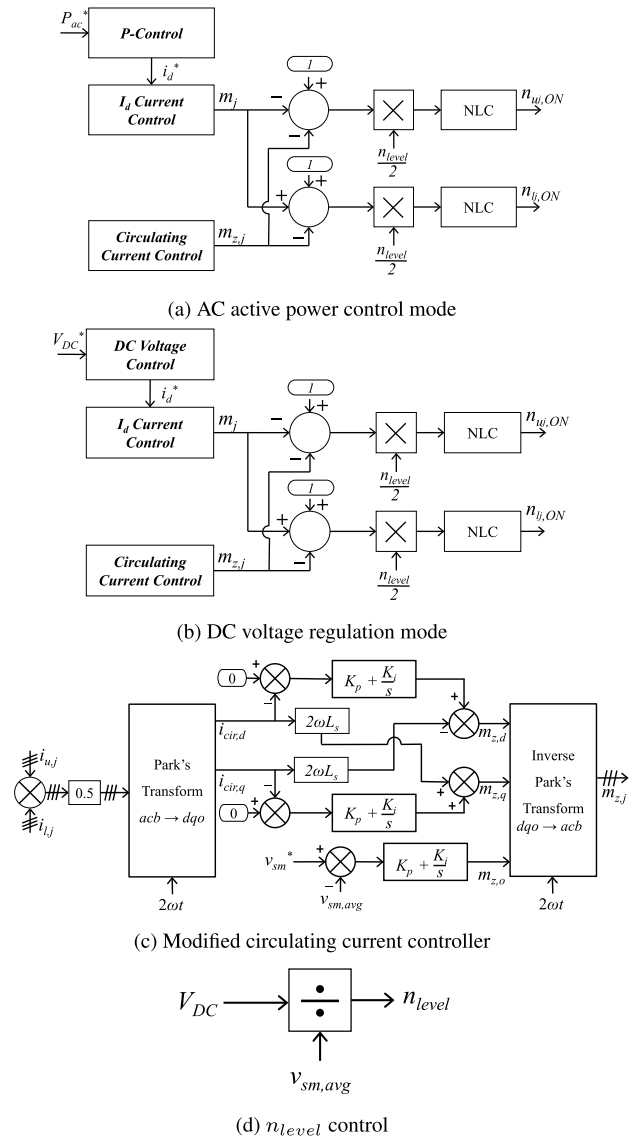


FIGURE 2. The structure of MMC controller to generate the number of ON submodule.

III. EXPLOITING THE SUBMODULE REDUNDANT ENERGY OF MMC–HVDC

A. THE RANGE OF n_{level} OF MMC–HVDC

Previous studies proposed inertia emulation control with VSC–HVDC using the energy buffer in the HVDC link [5], [8]. Those studies assumed that the VSC–HVDC is a 2-level or a 3-level converter. MMC is a representative topology of VSC at present, and this paper proposes n_{level} control for the inertia emulation control of MMC–HVDC. When VSC uses a $Y - \Delta$ transformer, the VSC can add a third-harmonic voltage to the modulation signal. The peak value of modulation signal can be increased from 1.0 to 1.15 [23], [43]. The third-harmonic injected modulation extends the range of n_{level} , which is obtained as follows:

$$N_{level} \leq n_{level} \leq K_n \times N_{level} \quad (8)$$

where K_n is a coefficient of the maximum n_{level} extension factor (1.265), which is obtained from the redundant factor

(1.1), multiplying third harmonic injection extension range (1.15). Here, N_{level} is the number of levels of MMC in normal operation. Note that n_{level} needs to be greater than N_{level} because the submodule IGBTs and capacitor have voltage limit.

B. MAXIMUM ENERGY AVAILABLE FOR n_{level} CONTROL OF MMC AND EQUIVALENT INERTIA CONSTANT

Based on the swing equation in the power system, the inertia constant H of synchronous machine can be described as follows [8]:

$$H = \frac{W_K}{S_{rated}} = \frac{J\omega_s^2}{2S_{rated}} \quad (9)$$

where W_K is the stored kinetic energy in MJ at synchronous speed, S_{rated} is the machine rating in MVA, J is the total moment of inertia of the rotor mass in $kg - m^2$, and ω_s is the synchronous speed of the machine. As the angular velocity decreases, the kinetic energy of the synchronous machine changes and the amount of the kinetic energy change (ΔW_K) is injected into the power system. The amount of the kinetic energy change can be obtained as follows:

$$\Delta W_K = \frac{J(\omega_0^2 - \omega_s^2)}{2} = \frac{J}{2}\omega_0^2 \left(1 - \frac{f_s^2}{f_0^2}\right) = K_f \cdot W_K \quad (10)$$

where $K_f = 1 - f_s^2/f_0^2$. ω_0 is the angular velocity of a synchronous machine corresponding to the fundamental frequency of the power system. Here, f_0 is the fundamental frequency of the power system in Hz , and f_s is the frequency of the synchronous machines in Hz . Additionally, f_s is equal to the frequency of the power system. It is worth mentioning that f_s varies. When the frequency has a lower limit, the maximum available kinetic energy can be obtained as follows:

$$\Delta W_{K,max} = \left(1 - \frac{f_{s,min}^2}{f_0^2}\right) \cdot W_K = K_{f,max} \cdot W_K \quad (11)$$

where $K_{f,max} = 1 - f_{s,min}^2/f_0^2$. The frequency $f_{s,min}$ is the lower frequency limit.

Similarly, MMC has the electrostatic energy in the submodule capacitors. The stored energy in MMC can be expressed as follows:

$$W_{MMC} = \frac{1}{2}C_{SM}v_{SM,avg}^2 \times (6N_{SM}) \quad (12)$$

$$= 3C_{SM}N_{SM} \frac{V_{DC}^2}{n_{level}^2} \quad (13)$$

The total number of submodules in MMC is $6N_{SM}$ because MMC has six arms. The maximum and minimum energy of MMC can be obtained in (14) and (15) because the minimum number of n_{level} is N_{level} and the maximum number of n_{level} is $K_n \cdot N_{level}$ in (8).

$$W_{MMC,max} = 3C_{SM}N_{SM} \frac{V_{DC}^2}{N_{level}^2} \quad (14)$$

$$W_{MMC,min} = 3C_{SM}N_{SM} \frac{V_{DC}^2}{K_n^2 \cdot N_{level}^2} \quad (15)$$

The maximum available electrostatic energy (ΔW_{MMC}) in MMC can be calculated using (16).

$$\begin{aligned} \Delta W_{MMC} &= W_{MMC,max} - W_{MMC,min} \\ &= \left(1 - \frac{1}{1.265^2}\right) \times W_{MMC,N_{level}} \\ &\approx 0.375 \times W_{MMC,N_{level}} \end{aligned} \quad (16)$$

where $K_n = 1.265$, as obtained in (8).

C. INERTIA CONSTANT OF n_{level} CONTROL OF MMC

The inertia constant of n_{level} control of MMC (H_{MMC}) can be obtained by equating the maximum available kinetic energy of the synchronous machine in (11) and the maximum available electrostatic energy of MMC in (16).

$$\Delta W_{MMC} = \Delta W_{K,max} \quad (17)$$

$$0.375 \times W_{MMC,N_{level}} \approx K_{f,max} \cdot W_K = K_{f,max} \cdot H \cdot S_{rated} \quad (18)$$

Let $S_{rated} = S_{MMC}$ and $H = H_{MMC}$. Then, H_{MMC} is then expressed as follows:

$$H_{MMC} \approx \frac{0.375 \times W_{MMC,N_{level}}}{K_{f,max} \cdot S_{MMC}} \quad (19)$$

The $f_{s,min}$ in $K_{f,max}$ gives the lower frequency limit of the frequency support control of the MMC. This means that $f_{s,min}$ is the frequency that supports maximum inertial energy. For example, if the frequency $f_{s,min}$ is set to be $59.2 Hz$, the frequency support control of MMC–HVDC is active within the range of $59.2 Hz$ to $60 Hz$. Although the energy stored in the MMC is limited and small, it is controllable. To utilize the energy to support the inertia of the power system, it is necessary to use stored energy efficiently. Thus, this paper sets $f_{s,min}$ to the lowest frequency allowed by the power system (e.g. under frequency load shedding (f_{UFLS})).

D. n_{level} CONTROL FOR FREQUENCY SUPPORT

The swing equation is given in (20).

$$\frac{2H}{f_0} \cdot \frac{df}{dt} = \Delta P_1 \quad (20)$$

where ΔP_1 is the power change of the synchronous machine in per-unit (pu) system. The power change of MMC can be expressed as a derivative of energy in pu:

$$\frac{6}{S_{MMC}} \cdot \frac{dE_{arm,avg}}{dt} = \frac{6C_{SM}N_{SM}v_{SM,avg}}{S_{MMC}} \cdot \frac{dv_{SM,avg}}{dt} = \Delta P_2 \quad (21)$$

where ΔP_2 is the power change of MMC in pu. Equating ΔP_1 and ΔP_2 yields (22).

$$\frac{2H_{MMC}}{f_0} \cdot \frac{df}{dt} = \frac{6C_{SM}N_{SM}v_{SM,avg}}{S_{MMC}} \cdot \frac{dv_{SM,avg}}{dt} \quad (22)$$

Integrating both sides of (22) yields:

$$\int \frac{2H_{MMC}}{f_0} \cdot \frac{df}{dt} = \int \frac{6C_{SM}N_{SM}v_{SM,avg}}{S_{MMC}} \cdot \frac{dv_{SM,avg}}{dt} \quad (23)$$

$$\frac{2H_{MMC} \cdot f}{f_0} = \frac{3C_{SM}N_{SM}v_{SM,avg}^2}{S_{MMC}} + K_1 \quad (24)$$

where $K_1 = 2H_{MMC} - 3C_{SM}N_{SM}V_{SM,avg}^2/S_{MMC}$.

The average submodule voltage corresponding to power system frequency (f) can then be obtained as follows:

$$\begin{aligned} v_{SM,avg} &= \sqrt{V_{SM,avg}^2 - \frac{2H_{MMC}S_{MMC} \cdot (f_0 - f)}{3C_{SM}N_{SM}f_0}} \\ &= \sqrt{\left(1 - \frac{0.75 \cdot (f_0 - f)}{K_{f,max} \cdot f_0}\right)} V_{SM,avg} \end{aligned} \quad (25)$$

Finally, n_{level} , as function of power system frequency, is achieved as follows:

$$n_{level} = \frac{V_{DC}}{v_{SM,avg}} \quad (26)$$

$$= \frac{V_{DC}}{\sqrt{K_2 \cdot V_{SM,avg}^2}} \quad (27)$$

$$= \frac{N_{level}}{\sqrt{K_2}} \quad (28)$$

where $K_2 = 1 - 0.75 \cdot (f_0 - f)/(K_{f,max} \cdot f_0)$.

Figure 3 illustrates the control diagram of the proposed n_{level} control for MMC–HVDC. The frequency can be obtained using phase-locked-loop (PLL). As the submodule voltage ($v_{sm,avg}$) decreases, the number of level (n_{level}) increases.

E. V_{DC} CONTROL FOR FREQUENCY SUPPORT

Using energy stored by DC line and cable for fast primary frequency control is proposed in [3]–[5], [8]. This paper also propose using charged energy in a DC line or cable. Equation (5) shows that as V_{DC} decreases, n_{level} also decreases. It is important noting that decreasing n_{level} allows more energy can be exploited from submodule. Therefore, the proposed V_{DC} control helps MMC exploit the redundant energy of MMC–HVDC and this is additional benefit when using V_{DC} control and n_{level} control for improved frequency response at the same time.

Like submodule redundancy V_{DC} also has margin to avoid overmodulation. As stated in Section III-A, VSC can add a third-harmonic voltage to the modulation signal and the peak value of modulation signal can be increased from 1.0 to 1.15 [23], [43]. This means that V_{DC} can be decreased to $V_{DC}/1.15$. Then, the maximum available energy from DC line can be calculated using (29).

$$\begin{aligned} \Delta W_{DCLine} &= W_{DCLine,max} - W_{DCLine,min} \\ &= \left(1 - \frac{1}{1.15^2}\right) \times W_{DCLine} \\ &\approx 0.243 \times W_{DCLine} \end{aligned} \quad (29)$$

where,

$$W_{DCLine} = 2 \times \frac{1}{2} C_{DCLine} \left(\frac{V_{DC}}{2}\right)^2$$

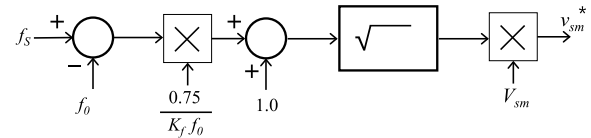


FIGURE 3. Block diagram of n_{level} control for frequency support to generate submodule voltage reference.

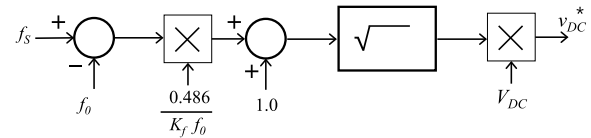


FIGURE 4. Block diagram of V_{DC} control for frequency support to generate DC voltage reference.

C_{DCLine} is the capacitance of DC line or cable. Note that C_{DCLine} is determined parameter, not controllable parameter. Equating ΔW_{DCLine} and $\Delta W_{K,max}$ yields (30).

$$\Delta W_{DCLine} = \Delta W_{K,max} \quad (30)$$

$$0.243 \times W_{DCLine} \approx K_{f,max} \cdot W_K = K_{f,max} \cdot H \cdot S_{rated} \quad (31)$$

Let $S_{rated} = S_{MMC}$ and $H = H_{DCLine}$. The inertia constant of DC line (H_{DCLine}) is then expressed as follows:

$$H_{DCLine} \approx \frac{0.243 \times W_{DCLine}}{K_{f,max} \cdot S_{MMC}} \quad (32)$$

The DC voltage reference corresponding to power system frequency (f) can then be obtained as follows:

$$\begin{aligned} v_{DC} &= \sqrt{V_{DC}^2 - \frac{2H_{DCLine}S_{MMC} \cdot (f_0 - f)}{0.5 \cdot C_{DCLine}f_0}} \\ &= \sqrt{\left(1 - \frac{0.486 \cdot (f_0 - f)}{K_{f,max} \cdot f_0}\right)} V_{DC} \end{aligned} \quad (33)$$

Figure 4 illustrates the control diagram of the proposed V_{DC} control of MMC–HVDC for frequency support.

IV. CASE STUDY

A. CONFIGURATION OF JEJU POWER SYSTEM FOR SIMULATION

The simplified schematic diagram of the Jeju Island transmission system, which is test system for the proposed method, is shown in Figure 5 [48]. The AC system of Jeju Island has two line-commuted converter (LCC)-HVDC inverters, two synchronous condensers (SC), eight synchronous generators, and multiple Wind Power Plants (WPPs). MMC–HVDC will be installed by 2020 and two Combined Cycle (C/C) generators (240 MW) will be installed in 2018 [2]. The rated capacity, minimum and maximum power, inertia of generators, and HVDC systems of the future Jeju power system are presented in Table 1. As the penetration level of wind power generation has been growing rapidly, severe stability problems in system frequency are likely to occur

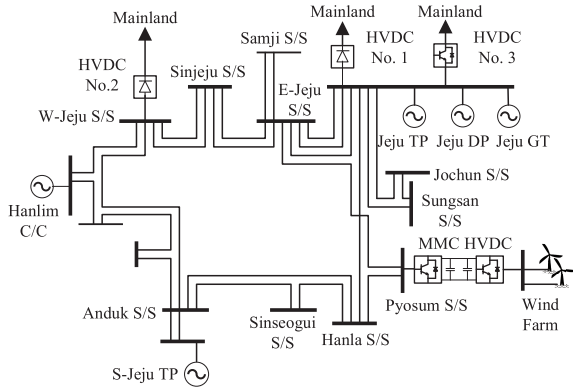


FIGURE 5. The schematic diagram of Jeju Island transmission system.

TABLE 1. Generators and HVDCs specification in Jeju power system.

Generators	P_{max} [MW]	P_{min} [MW]	Inertia constant [s]	Rating [MVA]
Jeju GT No.1 & No.2 (SC)	-	-	2.56	50
Jeju DP No.1 & No.2	40	26	6.71	44.96
S-Jeju TP No.3 & No.4	100	50	5.93	130
Jeju C/C No.1 & No.2	120	50	8.00	140
Jeju TP No.2 & No.3	75	42	5.4	97.06
Hanlim C/C	105	41	6.0	150
HVDC No.1 (LCC)	300	30	-	300
HVDC No.2 (LCC)	400	40	-	400
HVDC No.3 (MMC)	200	-200	-	210
Offshore Wind (MMC)	200	0	-	210
Onshore Wind	1100	-	-	1100

because this inverter-based distributed energy source is not able to provide sufficient inertia. Within the highly sensitive environment of Jeju Island, this study will show that the MMC–HVDC, installed to deliver power from the offshore WPPs and mainland, can support inertia and strengthen the stability of the system by exploiting an energy buffer based on the proposed n_{level} control. We select 2022 Jeju power system with the off-peak condition for the test system due to its high penetration level of converter based generation and transmission. This might be vulnerable to disturbances. The peak load level on Jeju Island is expected to be 1111 MW, and the off-peak load level is expected to be 603 MW in 2022 [2]. The total capacity of installed WPP is growing rapidly, and it is expected to reach 1.3 GW in 2022. HVDC systems and other generators are sufficient to satisfy the demand load.

We assume that 200 MW of capacity of the WPP and HVDC No.3 are connected to Jeju island grid through the MMC–HVDC system and HVDC No.3. The specification of the MMC–HVDC system is presented in Table 2. Each converter station has a 210 MVA capacity and 170 kV rated AC voltage. In normal operation, HVDC No.1 and HVDC No.3 transfer power from the mainland to Jeju to mitigate frequency deviation by employing droop control, the rate for which is set to be 5% in this paper. The frequency regulation controllers of HVDCs are illustrated in Figure 8 and the parameters are presented in Table 6. Additionally, MMC–HVDC systems provide power with the transmission system

TABLE 2. MMC specifications for normal operation.

System frequency	60 Hz
Rated apparent power	210 MVA
AC voltage	154 kV
Transformer	154 kV/170 kV (Y/Δ)
DC voltage (V_{DC})	±150 kV
Smoothing reactor	53 mH
Average submodule voltage ($V_{SM,avg}$)	2 kV
Submodule capacitance	3500 μF
DC cable capacitance	27.48 μF (100 km)
N_{SM}	165 per arm
N_{level}	150
W_{MMC}	6,930 kJ
W_{DCLine}	618.3 kJ
H_{MMC} (In case, $f_{s,min} = 59.2$ Hz)	0.467 s
H_{DCLine} (In case, $f_{s,min} = 59.2$ Hz)	0.027 s

TABLE 3. Generators in-service for the simulation (Off-peak load condition).

Generator	Amount of power [MW]	Amount of inertia [MW·s]
S-Jeju TP No.3 & 4	55	777.4 × 2
Jeju TP No.2	50	596.0
Wind-farm (MMC–HVDC)	105	0 ~ 201.8
Onshore WPPs (Type-3, DFIG)	215	0
HVDC No.1	75	0
HVDC No.3	48	0 ~ 201.8
Jeju GT No.1 & 2 (SC)	0	128 × 2
Total Load	603	-

instantaneously by fully utilizing its controllability based on the proposed n_{level} control and V_{DC} control for frequency support. We assume that the rectifier converter also provides inertia with n_{level} control to improve the frequency response of the Jeju power system using communication link between rectifier and inverter. Thus, 4 MMC and two HVDC cables provide inertia to Jeju power system when the frequency drops.

To verify the proposed frequency support control of MMC–HVDC for improved frequency response, the equivalent model of the Jeju Island transmission system is designed as shown in Figure 5 using PSCAD/EMTDC and E-TRAN. The off-peak load scenario is chosen to validate the proposed method because the number of in-service generators with the off-peak load condition is less than those with the peak load condition. Fewer in-service generators means that the power system has lower inertia. The generators condition of the simulation is presented in Table 3. The power rating of Jeju HVDC No. 1 is 300 MW with ±180 kV DC voltage and the power rating of HVDC No. 2 is 400 MW with ±250 kV DC voltage. HVDC No. 2 is not in service due to this scenario is off-peak condition. The rectifier of MMC–HVDC will transfer active power, and the inverter of MMC–HVDC will operate in DC voltage regulation mode in the simulation. For an $N - 1$ contingency in the Jeju Island power system with off-peak condition, we assume 95 MW of multiple onshore WPPs outage at 1 s. The simulations are divided into three cases according to H_{MMC} and H_{DCLine}

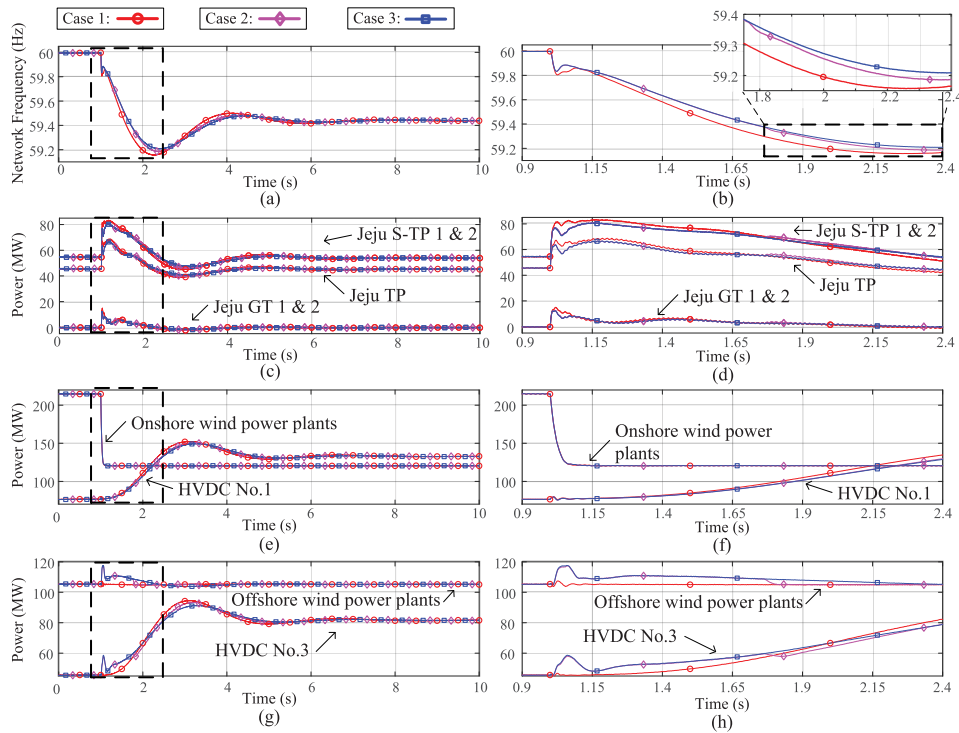


FIGURE 6. Power system frequency and dynamic responses of synchronous machines and HVDCs; (a) Network frequency, (b) network frequency (Zoom), (c) active power of synchronous machines, (d) active power of synchronous machines (Zoom), (e) active power of converter-based generation and transmission, (f) active power of converter-based generation and transmission (Zoom), (g) active power of MMC–HVDCs, (h) active power of MMC–HVDCs (Zoom).

TABLE 4. The simulation scenarios of MMC–HVDC.

Cases	$f_{s,min}$ [Hz]	H_{MMC} [s]	H_{DCLine} [s]	Total inertia of power system [MW·s]
Case 1	Disable	-	-	2406.8
Case 2	59.2	1.8687	-	2799.2
Case 3	59.2	1.8687	0.054	2810.5

of MMC–HVDC, as presented in Table 4. The rectifier of MMC–HVDC is also designed to provide inertia through DC connection. Therefore, H_{MMC} is quadrupled for the simulation since four MMCs participate in n_{level} control and H_{DCLine} is doubled for the simulation since two 100 km of DC cable are used in the simulation. The amounts of inertia of MMC and DC line for the simulation cases are presented in Table 4.

B. SIMULATION RESULT AND ANALYSIS

Figure 6 presents network frequency, active power responses of synchronous generators, synchronous condensers, onshore WPPs, HVDC No.1, and MMC–HVDCs during 95 MW of WPP outage. Figures 6(a) and (b) show that the proposed n_{level} control of MMC–HVDC reduces ROCOF and improves the frequency response. The ROCOFs for 500 ms from the outage are improved in Case 2 and Case 3 because the proposed MMC control injects power to Jeju power system. Note that Case 2 and Case 3 has almost same ROCOF (See Table 5) because Case 2 and Case 3 has similar inertia constant. The frequency is stabilized at 59.43 Hz for all cases.

The frequency dips (Nadir) are 59.1569 Hz for Case 1, 59.1852 Hz for Case 2, and 59.2077 Hz for Case 3 as presented in Table 5. This means that only Case 3 can avoid under frequency load shedding. As can be seen in Figures 6(c) and (d), synchronous generators and synchronous condensers provide inertia when the 95 MW of power is disappeared. Figures 6(e) and (f) shows that 95 MW of onshore wind power is tripped at 1 s and WPPs and HVDC No. 1 don’t provide inertia due to no inertia emulation control is applied for the simulation. After WPPs’ outage, HVDC No. 1 and No. 3 replenish the insufficient power due to onshore WPPs power interruption. Figures 6(g) and (h) present the active power of MMC–HVDCs for the three cases presented in Table 4. MMC–HVDC does not provide inertia for Case 1. Contrary to Case 1, MMC–HVDC provides inertia for Case 2 and Case 3. The dynamic responses of power of Case 2 and Case 3 are very similar because Case 2 and Case 3 has almost same inertia constant.

Figure 7 MMC–HVDC DC voltages of MMC inverters, the average submodule voltages of each MMC rectifiers and inverters, n_{level} of each MMC, and maximum number of ON submodule per Arm for MMCs. Figure 7(a) shows that DC voltage does not change and is maintained at 300 kV for Case 1 and Case 2 and DC voltage is controlled to the designed response for Case 3. In Figure 7(b), each of the four MMC submodule voltages are superimposed and appear as one. While the submodule voltages are controlled

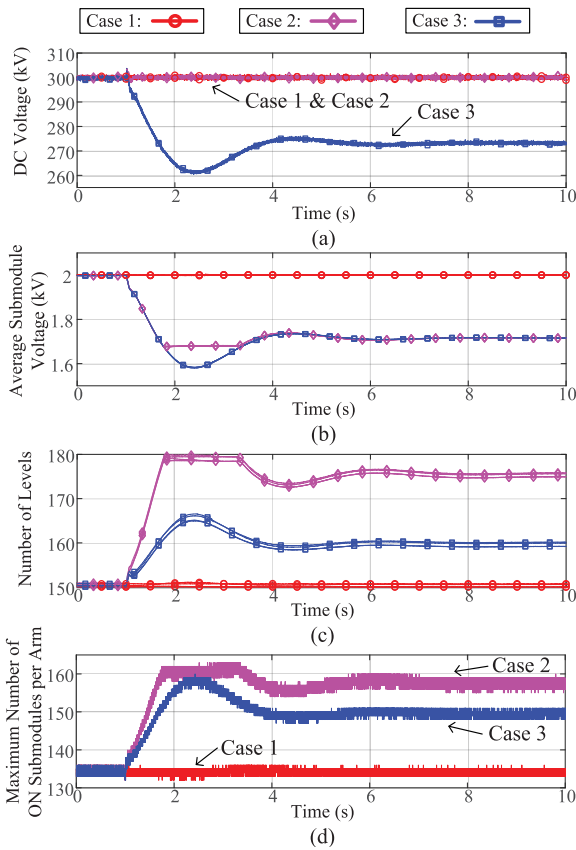


FIGURE 7. Dynamic responses of MMC–HVDC; (a) MMC–HVDC DC voltage, (b) average submodule voltages, (c) n_{level} of MMC–HVDC, (d) maximum number of ON submodules per arm of MMCs.

TABLE 5. The simulation results.

	ROCOF [Hz/s]	<i>Nadir</i> [Hz]	Maximum n_{level}	Maximum Number of ON Submodule per Arm
Case 1	1.0218	59.1569	151	137
Case 2	0.8960	59.1852	179	163
Case 3	0.8920	59.2077	166	161

to the desired value with AC-DC decoupled control (See Section II-C), the number of levels are different from each inverters and rectifiers (See Figure 7(c)) because the DC voltage of the inverters are different from that of the rectifiers. The submodule voltage decreases, and the number of levels of the MMC–HVDC increases. The maximum n_{level} are 151 for Case 1, 179 for Case 2, and 166 for Case 3. The maximum numbers of ON submodule per arm are 137 for Case 1, 163 for Case 2, and 161 for Case 3. The simulation results are summarized in Table 5.

C. DISCUSSION FOR DYNAMIC RESPONSE OF MMC BETWEEN 1.74 s AND 3.5 s

As presented in Table 4, total amounts of inertia of the power system for Case 2 and Case 3 are almost same. This is why the frequency response of Case 2 and Case 3 are almost the same from 1 s to 1.74 s. However, Figure 7(d) shows that maximum

ON submodule per arm of Case 2 goes to limit at 1.74 s. Although n_{level} can increase to 190 theoretically, n_{level} is limited to 180 in Case 2. This is because MMC inner dynamics requires additional modulation signal to suppress double line frequency circulating current during the power transfer. Because the magnitude of the additional modulation signal of MMC is proportional to the amount of power transmission, the MMC–HVDC transmits the lower power, the limit of level is high, and the MMC–HVDC transmits the higher power, the limit of levels is low. Thus, in Case 2, the average submodule voltage could not be lowered to 1.68 kV or less for the simulation and the energy from MMC could no longer be provided as shown in Figure 7(b). In Figure 6(h), the MMC–HVDCs stop providing inertia power at 1.74 s in Case 2 and then, the ROCOF is changed as can be seen in Figure 6(b). However, Case 3, which is the case that proposed n_{level} control and V_{DC} control are used at the same time, doesn't have inertia power interruption. Therefore, using n_{level} control and V_{DC} control together helps MMC exploit the redundant energy of MMC–HVDC and improves frequency response of the power system.

V. CONCLUSION

This paper proposes n_{level} control of MMC–HVDC to improve frequency response of a low-inertia AC grid by changing the number of levels in MMC control and thus providing the extra power to the grid in need. The inertia time constant of MMC (H_{MMC}) is quantified by associating the maximum available energy of MMC (ΔW_{MMC}) with the inertia energy of the synchronous machine ($\Delta W_{K,max}$). The rectifier can also be controlled to provide the similar inertial power as required. It thus literally mimics the inertial response of the synchronous machine and naturally provides the energy buffer to the system. In addition, the system planners and operators will benefit from knowing the amount of inertia from the MMC in situations where converter-based power generation increases and inertia of a power system declines. Two MMC–HVDC systems of this paper are designed to transfer the power from the offshore WPPs and the mainland to the Jeju power grid under off-peak loading condition where one LCC–HVDC, three generators, and two synchronous condensers are in service. The $N - 1$ contingency makes the Jeju power grid highly weak in terms of frequency stability and the proposed MMC inertial response is highly beneficial especially when the penetration level of renewable is high. The study results demonstrate that the proposed n_{level} control enables the autonomous inertial response of the MMC–HVDC along with the synchronous machines and improves the frequency response of low inertia power system. This contribution should become more crucial as the MMC is expected to achieve increased deployment in the future and form the multi-terminal DC grids to integrate more renewable energy sources.

APPENDIX

See Figure 8 and Tables 6 and 7.

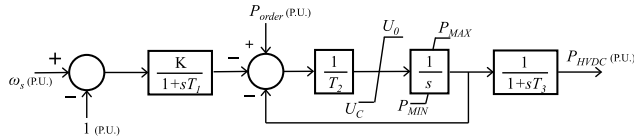


FIGURE 8. Frequency regulation controller of HVDCs in the simulation.

TABLE 6. Frequency regulation controller parameters in the simulation.

K	T_1	T_2	T_3	U_C	U_0
20	0.2	0.25	0.3	-0.3	0.3

TABLE 7. Parameters for generators and synchronous condensers.

Machine Constant	S-Jeju TP	Jeju TP	Jeju GT
X_d	1.68 [pu]	1.456 [pu]	1.94 [pu]
X_q	1.71 [pu]	1.405 [pu]	1.92 [pu]
X'_d	0.18 [pu]	0.206 [pu]	0.226 [pu]
X'_q	0.35 [pu]	0.5 [pu]	0.402 [pu]
$X''_d = X''_q$	0.13 [pu]	0.147 [pu]	0.172 [pu]
T'_{d0}	11.3 [s]	3.735 [s]	10.4 [s]
T'_{q0}	1.14 [s]	0.305 [s]	0.83 [s]

ACKNOWLEDGMENT

We thank Dr. Willem Leterme at KU Leuven and Mr. Dongsu Lee at Hyosung for sharing their knowledge with us. We would also like to thank anonymous reviewers for their comments that greatly improved the manuscript.

REFERENCES

[1] P. Tielens and D. Van Hertem, “The relevance of inertia in power systems,” *Renew. Sustain. Energy Rev.*, vol. 55, pp. 999–1009, Mar. 2016. doi: 10.1016/j.rser.2015.11.016.

[2] Ministry of Trade, Industry and Energy of the Republic of Korea, *8th Power Supply and Demand Plan for Korean Power System*, Power Sys. Planning Dept., Seoul, South Korea, Dec. 2017.

[3] B. Silva, C. L. Moreira, L. Seca, Y. Phulpin, and J. A. P. Lopes, “Provision of inertial and primary frequency control services using offshore multi-terminal HVDC networks,” *IEEE Trans. Sustain. Energy*, vol. 3, no. 4, pp. 800–808, Oct. 2012. doi: 10.1109/TSTE.2012.2199774.

[4] O. D. Adeuyi, M. Cheah-Mane, J. Liang, N. Jenkins, Y. Wu, C. Li, and X. Wu, “Frequency support from modular multilevel converter based multi-terminal HVDC schemes,” in *Proc. IEEE PES GM*, Denver, CO, USA, Jul. 2015, pp. 1–5.

[5] A. Junyent-Ferré, Y. Pipelzadeh, and T. C. Green, “Blending HVDC-link energy storage and offshore wind turbine inertia for fast frequency response,” *IEEE Trans. Sustain. Energy*, vol. 6, no. 3, pp. 1059–1066, Jul. 2015. doi: 10.1109/TSTE.2014.2360147.

[6] I. M. Sanz, P. D. Judge, C. E. Spallarossa, B. Chaudhuri, and T. C. Green, “Dynamic overload capability of VSC HVDC interconnections for frequency support,” *IEEE Trans. Energy Convers.*, vol. 32, no. 4, pp. 1544–1553, Dec. 2017. doi: 10.1109/TEC.2017.2712909.

[7] C. E. Spallarossa, M. M. C. Merlin, and T. C. Green, “Augmented inertial response of multi-level converters using internal energy storage,” in *Proc. IEEE Int. Energy Conf. (ENERGYCON)*, Apr. 2016, pp. 1–6.

[8] J. Zhu, C. D. Booth, G. P. Adam, A. J. Roscoe, and C. G. Bright, “Inertia emulation control strategy for VSC-HVDC transmission systems,” *IEEE Trans. Power Syst.*, vol. 28, no. 2, pp. 1277–1287, May 2013. doi: 10.1109/TPWRS.2012.2213101.

[9] J. Ekanayake and N. Jenkins, “Comparison of the response of doubly fed and fixed-speed induction generator wind turbines to changes in network frequency,” *IEEE Trans. Energy Convers.*, vol. 19, no. 4, pp. 800–802, Dec. 2004. doi: 10.1109/TEC.2004.827712.

[10] J. Morren, J. Pierik, and S. W. H. de Haan, “Inertial response of variable speed wind turbines,” *Electr. Power Syst. Res.*, vol. 76, no. 11, pp. 980–987, 2006. doi: 10.1016/j.epsr.2005.12.002.

[11] J. Morren, S. W. H. de Haan, W. L. Kling, and J. A. Ferreira, “Wind turbines emulating inertia and supporting primary frequency control,” *IEEE Trans. Power Syst.*, vol. 21, no. 1, pp. 433–434, Feb. 2006. doi: 10.1109/TPWRS.2005.861956.

[12] G. Ramtharan, J. B. Ekanayake, and N. Jenkins, “Frequency support from doubly fed induction generator wind turbines,” *IET Renew. Power Generation*, vol. 1, no. 1, pp. 3–9, Mar. 2007. doi: 10.1049/iet-rpg:20060019.

[13] R. G. de Almeida and J. A. Peças Lopes, “Participation of doubly fed induction wind generators in system frequency regulation,” *IEEE Trans. Power Syst.*, vol. 22, no. 3, pp. 944–950, Aug. 2007. doi: 10.1109/TPWRS.2007.901096.

[14] J. F. Conroy and R. Watson, “Frequency response capability of full converter wind turbine generators in comparison to conventional generation,” *IEEE Trans. Power Syst.*, vol. 23, no. 2, pp. 649–656, May 2008. doi: 10.1109/TPWRS.2008.920197.

[15] Z. Miao, L. Fan, D. Osborn, and S. Yuvarajan, “Wind farms with HVDC delivery in inertial response and primary frequency control,” *IEEE Trans. Energy Convers.*, vol. 25, no. 4, pp. 1171–1178, Dec. 2010. doi: 10.1109/TEC.2010.2060202.

[16] I. D. Margaris, S. A. Papatthanassiou, N. D. Hatziaargyriou, A. D. Hansen, and P. Sorensen, “Frequency control in autonomous power systems with high wind power penetration,” *IEEE Trans. Sustain. Energy*, vol. 3, no. 2, pp. 189–199, Apr. 2012. doi: 10.1109/TSTE.2011.2174660.

[17] H. Lee, J. Kim, D. Hur, and Y. C. Kang, “Inertial control of a DFIG-based wind power plant using the maximum rate of change of frequency and the frequency deviation,” *J. Electr. Eng. Technol.*, vol. 10, no. 2, pp. 496–503, Mar. 2015. doi: 10.5370/JEET.2015.10.2.496.

[18] M. Hwang, Y. H. Chun, J. W. Park, and Y. C. Kang, “Dynamic droop-based inertial control of a wind power plant,” *J. Electr. Eng. Technol.*, vol. 10, no. 3, pp. 1363–1369, May 2015. doi: 10.5370/JEET.2015.10.3.1363.

[19] M. Hwang, E. Muljadi, J.-W. Park, P. Sørensen, and Y. C. Kang, “Dynamic droop-based inertial control of a doubly-fed induction generator,” *IEEE Trans. Sustain. Energy*, vol. 7, no. 3, pp. 924–933, Jul. 2016. doi: 10.1109/TSTE.2015.2508792.

[20] J. Lee, E. Muljadi, P. Srensen, and Y. C. Kang, “Releasable kinetic energy-based inertial control of a DFIG wind power plant,” *IEEE Trans. Sustain. Energy*, vol. 7, no. 1, pp. 279–288, Jan. 2016. doi: 10.1109/TSTE.2015.2493165.

[21] G. T. Son, H. Lee, T. Nam, Y. Chung, U. Lee, S. Baek, K. Hur, and J. Park, “Design and control of a modular multilevel HVDC converter with redundant power modules for noninterruptible energy transfer,” *IEEE Trans. Power Del.*, vol. 27, no. 3, pp. 1611–1619, Jul. 2012. doi: 10.1109/TPWRD.2012.2190530.

[22] G. Konstantinou, J. Pou, S. Ceballos, and V. G. Agelidis, “Active redundant submodule configuration in modular multilevel converters,” *IEEE Trans. Power Del.*, vol. 28, no. 4, pp. 2333–2341, Oct. 2013. doi: 10.1109/TPWRD.2013.2264950.

[23] J. Kang, H. Kim, H.-J. Jung, D.-S. Lee, C.-K. Kim, H. A. Mantooh, and K. Hur, “On exploiting active redundancy of a modular multilevel converter to balance reliability and operational flexibility,” *IEEE Trans. Power Electron.*, vol. 34, no. 3, pp. 2234–2243, Mar. 2019. doi: 10.1109/TPEL.2018.2846406.

[24] G. Liu, Z. Xu, Y. Xue, and G. Tang, “Optimized control strategy based on dynamic redundancy for the modular multilevel converter,” *IEEE Trans. Power Electron.*, vol. 30, no. 1, pp. 339–348, Jan. 2015. doi: 10.1109/TPEL.2014.2305663.

[25] K. Ilves, A. Antonopoulos, L. Harnefors, S. Norrga, L. Angquist, and H. P. Nee, “Capacitor voltage ripple shaping in modular multilevel converters allowing for operating region extension,” in *Proc. 37th Annu. Conf. IEEE Ind. Electron. Soc. (IECON)*, Nov. 2011, pp. 4403–4408.

[26] M. Vasiladiotis, N. Cherix, and A. Rufer, “Accurate capacitor voltage ripple estimation and current control considerations for grid-connected modular multilevel converters,” *IEEE Trans. Power Electron.*, vol. 29, no. 9, pp. 4568–4579, Sep. 2014. doi: 10.1109/TPEL.2013.2286293.

[27] M. Zygmanski, B. Grzesik, and R. Nalepa, “Capacitance and inductance selection of the modular multilevel converter,” in *Proc. 15th Eur. Conf. Power Electron. Appl. (EPE)*, 2013, pp. 1–10.

[28] K. Ilves, S. Norrga, L. Harnefors, and H.-P. Nee, “On energy storage requirements in modular multilevel converters,” *IEEE Trans. Power Electron.*, vol. 29, no. 1, pp. 77–88, Jan. 2014. doi: 10.1109/TPEL.2013.2254129.

[29] H. Kim, S. Kim, Y.-H. Chung, D.-W. Yoo, C.-K. Kim, and K. Hur, “Operating region of modular multilevel converter for HVDC with controlled second-order harmonic circulating current: Elaborating P-Q capability,” *IEEE Trans. Power Del.*, vol. 31, no. 2, pp. 493–502, Apr. 2016. doi: 10.1109/TPWRD.2015.2458038.

- [30] K. Sharifabadi, L. Harnefors, H.-P. Nee, S. Norrga, and R. Teodorescu, *Design, Control, and Application of Modular Multilevel Converters for HVDC Transmission Systems*. Chichester, U.K.: Wiley, 2016.
- [31] U. N. Gnanarathna, A. M. Gole, and R. P. Jayasinghe, "Efficient modeling of modular multilevel HVDC converters (MMC) on electromagnetic transient simulation programs," *IEEE Trans. Power Del.*, vol. 26, no. 1, pp. 316–324, Jan. 2011. doi: [10.1109/TPWRD.2010.2060737](https://doi.org/10.1109/TPWRD.2010.2060737).
- [32] H. Saad, S. Denetiere, J. Mahseredjian, P. Delarue, X. Guillaud, J. Peralta, and S. Nguefeu, "Modular multilevel converter models for electromagnetic transients," *IEEE Trans. Power Del.*, vol. 29, no. 3, pp. 1481–1489, Jun. 2014. doi: [10.1109/TPWRD.2013.2285633](https://doi.org/10.1109/TPWRD.2013.2285633).
- [33] J. Xu, C. Zhao, W. Liu, and C. Guo, "Accelerated model of modular multilevel converters in PSCAD/EMTDC," *IEEE Trans. Power Del.*, vol. 28, no. 1, pp. 129–136, Jan. 2013. doi: [10.1109/TPWRD.2012.2201511](https://doi.org/10.1109/TPWRD.2012.2201511).
- [34] H. Kim, S. Jung, F. Mosallat, and K. Hur, "Validation for Compatible modular multilevel converter models using PSCAD/EMTDC," in *Proc. Asia-Pacific Power Energy Eng. Conf. (APPEEC)*, Hong Kong, Dec. 2013, pp. 1–6.
- [35] M. Saeedifard and R. Iravani, "Dynamic performance of a modular multilevel back-to-back HVDC system," *IEEE Trans. Power Del.*, vol. 25, no. 4, pp. 2903–2912, Oct. 2010. doi: [10.1109/TPWRD.2010.2050787](https://doi.org/10.1109/TPWRD.2010.2050787).
- [36] Q. Tu, Z. Xu, and L. Xu, "Reduced switching-frequency modulation and circulating current suppression for modular multilevel converters," *IEEE Trans. Power Del.*, vol. 26, no. 3, pp. 2009–2017, Jul. 2011. doi: [10.1109/TPWRD.2011.2115258](https://doi.org/10.1109/TPWRD.2011.2115258).
- [37] E. Solas, G. Abad, J. A. Barrena, S. Aurtinetxea, A. Carcar, and L. Zajac, "Modular multilevel converter with different submodule concepts—Part I: Capacitor voltage balancing method," *IEEE Trans. Ind. Electron.*, vol. 60, no. 10, pp. 4525–4535, Oct. 2013. doi: [10.1109/TIE.2012.2210378](https://doi.org/10.1109/TIE.2012.2210378).
- [38] T. Nam, H. Kim, S. Kim, G. T. Son, Y. H. Chung, J. Park, C. Kim, and K. Hur, "Trade-off strategies in designing capacitor voltage balancing schemes for modular multilevel converter HVDC," *J. Electr. Eng. Technol.*, vol. 11, no. 4, pp. 1921–1930, Jul. 2016. doi: [10.5370/JEET.2016.11.4.829](https://doi.org/10.5370/JEET.2016.11.4.829).
- [39] H. Saad, X. Guillaud, J. Mahseredjian, S. Denetiere, and S. Nguefeu, "MMC capacitor voltage decoupling and balancing controls," *IEEE Trans. Power Del.*, vol. 30, no. 2, pp. 704–712, Apr. 2015. doi: [10.1109/TPWRD.2014.2338861](https://doi.org/10.1109/TPWRD.2014.2338861).
- [40] S. Cui, S. Kim, J.-J. Jung, and S.-K. Sul, "A comprehensive cell capacitor energy control strategy of a modular multilevel converter (MMC) without a stiff DC bus voltage source," in *Proc. IEEE Appl. Power Electron. Conf. Expo. (APEC)*, Fort Worth, TX, USA, Mar. 2014, pp. 602–609.
- [41] A. Anlonopoulos, L. Angquist, and H. P. Nee, "On dynamics and voltage control of the modular multilevel converter," in *Proc. 13th Eur. Conf. Power Electron. Appl. (EPE)*, 2009, pp. 1–10.
- [42] J. Rodriguez, L. Franquelo, S. Kouro, J. Leon, R. Portillo, M. Prats, and M. Perez, "Multilevel converters: An enabling technology for high-power applications," *Proc. IEEE*, vol. 97, no. 11, pp. 1786–1817, Nov. 2009. doi: [10.1109/JPROC.2009.2030235](https://doi.org/10.1109/JPROC.2009.2030235).
- [43] A. Yazdani and R. Iravani, *Voltage-Sourced Converters in Power Systems: Modeling, Control, and Applications*. Hoboken, NJ, USA: Wiley, 2010.
- [44] H. Gu, R. Yan, and T. K. Saha, "Minimum synchronous inertia requirement of renewable power systems," *IEEE Trans. Power Syst.*, vol. 33, no. 2, pp. 1533–1543, Mar. 2018. doi: [10.1109/TPWRS.2017.2720621](https://doi.org/10.1109/TPWRS.2017.2720621).
- [45] *Integrating Renewable Energy—Wind Integration Studies Report*, Austral. Energy Market Operator, Melbourne, VIC, Australia, 2013.
- [46] *Future Power System Security Program—Progress Report*, Austral. Energy Market Operator, Melbourne, VIC, Australia, Jan. 2017.
- [47] *RoCoF—An Independent Analysis on the Ability of Generators to Ride Through Rate of Change of Frequency Values up to 2Hz/s*, DNV KEMA, Arnhem, The Netherlands, Feb. 2013.
- [48] M. Yoon, Y.-T. Yoon, and G. Jang, "A study on maximum wind power penetration limit in island power system considering high-voltage direct current interconnections," *Energies*, vol. 8, no. 12, pp. 14244–14259, Dec. 2015. doi: [10.3390/en8121425](https://doi.org/10.3390/en8121425).

• • •